J. Fluid Mech. (1997), *vol.* 338, *pp.* 387–410

On the behaviour of a fluid-loaded cylindrical shell with mean flow

By N. PEAKE

Department of Applied Mathematics and Theoretical Physics, University of Cambridge, Silver Street, Cambridge CB3 9EW, UK

(Received 14 November 1996 and in revised form 3 January 1997)

The unsteady behaviour of an infinitely long fluid-loaded elastic plate which is driven by a single-frequency point-force excitation in the presence of mean flow is known to exhibit a number of unexpected features, including absolute instability when the normalized flow speed, U, lies above some critical speed U_0, and certain unusual propagation effects for $U < U_0$. In the latter respect Crighton & Oswell (1991) have demonstrated most significantly that for a particular frequency range there exists an anomalous neutral (negative energy) mode which has group velocity pointing towards the driver, in violation of the usual radiation condition of outgoing waves at infinity. They show that the rate of working of the driver can be negative, due to the presence of other negative-energy waves, and can also become infinite at a critical frequency corresponding to a real modal coalescence. In this paper we attempt to extend these results by including, as is usually the case in a practical situation, plate curvature in the transverse direction, by considering a fluid-loaded cylinder with axial mean flow. In the limit of infinite normalized cylinder radius, a, Crighton & Oswell's results are regained, but for finite a very significant modifications are found. In particular, we demonstrate that the additional stiffness introduced by the curvature typically moves the absolute-instability boundary to a much higher flow speed than for the flat-plate case. Below this boundary we show that Crighton & Oswell's anomalous neutral mode can only occur for $a > a_1(U)$, but in practical situations it turns out that $a_1(U)$ is exceedingly large, and indeed seems much larger than radii of curvature achievable in engineering practice. Other negative-energy waves are seen to exist down to a smaller, but still very large, critical radius $a_2(U)$, while the existence of a real modal coalescence point, leading to a divergence in the driver admittance, occurs down to a slightly smaller critical radius $a_3(U)$. The transition through these various flow regimes as U and a vary is fully described by numerical investigation of the dispersion relation and by asymptotic analysis in the (realistic) limit of small U. The inclusion of plate dissipation is also considered, and, in common with Abrahams & Wickham (1994) for the flat plate, we show how the flow then becomes absolutely unstable at all flow speeds provided that $a > a_2(U)$.

1. Introduction

The interaction between an elastic structure and the surrounding fluid is an essential consideration in the design of almost all large-scale engineering structures, especially for marine applications where the level of 'fluid loading' can be particularly significant. Of great concern is the effect of structural inhomogeneities, such as rivets, which can

transmit vibrations from nearby machinery into the coupled fluid–solid system, leading at the very least to noise and fatigue problems and possibly even to the development of potentially damaging instabilities. Indeed, the whole question of the excitation and subsequent development of (for instance, flutter-type) instabilities in such systems has attracted, and continues to attract, considerable attention. From a fundamental and theoretical point of view, we mention here the early work of Benjamin (1960, 1963) and Landahl (1962), who were concerned with the unsteady behaviour of an incompressible fluid flow over an infinite compliant surface (extensions to more realistic Kramer surfaces have been undertaken by, for instance, Carpenter & Garrad 1985, 1986). A particular feature of such systems is the existence of negative-energy waves, whose excitation can lead to a decrease in the system energy and which are destabilized by plate dissipation or fluid viscosity (see Cairns 1979 for further details).

Following on from this earlier work, recent research has indicated the possibility of even more unexpected and unusual behaviour. The (deceptively simple) basic model problem is to determine the causal long-time behaviour of an infinite, two-dimensional elastic plate with non-zero mean flow on one side, driven by a single-frequency point force. This problem was studied by Brazier-Smith & Scott (1984), essentially via a numerical investigation of the unforced dispersion relation, and then in very great detail analytically by Crighton & Oswell (1991). Both sets of authors used the spatial instability theory developed first in plasma physics by Briggs (1964) and Bers (1983), and were able to show that the flow is in fact absolutely unstable for flow speeds in excess of a critical value U_0 (which Crighton & Oswell determined in closed form). For flow speeds less than U_0, however, highly unusual propagation effects were seen to occur, and in particular Crighton & Oswell identify an anomalous neutral mode which, over a narrow range of frequencies ($\omega_s < \omega < \omega_p$ say), is found downstream of the driver but with a negative group velocity (i.e. a group velocity directed towards the driver), in violation of the usual outgoing-wave radiation condition. This behaviour is shown to be a consequence of the fact that the driver is not the only source of energy in the system, and that the wave disturbances can act so as to extract energy from the mean flow. Indeed, Crighton & Oswell demonstrate that the mean rate of working of the driver, as measured by the real part of the line admittance, is positive for $\omega > \omega_p$, but is negative both in their anomalous propagation range $\omega_s < \omega < \omega_p$ and in the frequency range $0 < \omega < \omega_s$ over which the flow is convectively unstable. Also, the driver admittance becomes infinite at $\omega = \omega_p$, corresponding to a modal coalescence (or 'pinch') on the real k-axis. It must be emphasized that these effects are entirely to be associated with the presence of mean flow – when the mean-flow speed is zero, all modes have group velocity directed away from the driver, and the mean rate of working of the driver is always positive.

The way in which such an apparently simple problem can exhibit such unusual behaviour has excited quite considerable interest. For instance, Abrahams & Wickham (1994) have used largely analytical techniques to study the same infinite-plate problem as Crighton & Oswell (1991), but with additional features such as plate dissipation, modified plate equations and mean shear. Their findings seem to confirm Crighton & Oswell's results, but also indicate additional unusual behaviour, including the fact that once plate dissipation is included the flow becomes absolutely unstable for all mean-flow speeds. Also, Wu & Maestrello (1995), Lucey & Carpenter (1992) and Lucey (1996) have examined the case of a finite elastic baffle in a rigid plane with mean flow, and although these investigations have been

completed numerically, so that direct comparison with Crighton & Oswell's (1991) results is difficult, it does seem that significant differences from the infinite case can arise.

In this paper we aim to pursue Abrahams & Wickham's idea of extending the Crighton & Oswell (1991) infinite-plate analysis, but here to include the effects of transverse plate curvature, and this seems to be a problem of particular relevance, since the wave motions typically have long wavelengths which must be at least comparable to the radii of curvature found in many engineering structures. In physical terms, the transverse plate curvature will essentially introduce a second (hoop) stiffness into the Crighton–Oswell problem, and we will see that this will produce very significant modifications to the flat-plate dynamics, even for exceedingly small amounts of curvature. Specifically, we consider here an infinitely long elastic cylinder with uniform axial mean flow either externally or internally, which is driven by a time-harmonic ring force of fixed azimuthal mode number. The motion of a fluid-loaded cylindrical shell with mean flow has been studied extensively, for instance in a very thorough investigation of the dispersion relation by Scott (1988), and in terms of the acoustic radiation properties by Zhang & Abrahams (1995) and Guo (e.g. 1996). The behaviour of collapsible tubes with flow has also been studied extensively, particularly in the context of pulmonary flow (see for instance the review by Grotberg 1994). Also, Triantafyllou (1992) has studied the absolute instability of a very thin cylindrical beam placed in an external flow using slender body theory. However, it seems that the sort of dispersion-relation analysis carried out by Crighton & Oswell for the flat plate has not been performed for a thin cylindrical shell with mean flow, and that will therefore be the subject of the present paper.

In §2 we describe the mathematical formulation and solution of the problem, and outline the Briggs–Bers method used to determine the causal long-time limit of the initial value problem. In §3 we then investigate the conditions required for absolute instability – in the limit of infinite cylinder radius the Crighton & Oswell result is regained, but for finite (but still large) cylinder radius the minimum value of flow speed required for absolute instability is increased very significantly, and apparently well beyond the speed ranges encountered in typical underwater applications. For small values of U we present an implicit expression for the absolute instability boundary. In §4 we then investigate the behaviour of the system below this critical flow speed. Most strikingly, we show that Crighton & Oswell's anomalous mode with inward-pointing group velocity is eliminated by even a small amount of curvature; for instance, for steel in water with a typical flow speed we find that the anomalous propagation effect is only present when the plate radius of curvature is greater than about 166 000 plate thicknesses, which seems to be a degree of flatness which is not attained in engineering practice! Specifically, we uncover a sequence of critical radii $a_1(U) > a_2(U) > a_3(U)$: for $a < a_1(U)$ the anomalous mode mentioned above cannot occur, for $a < a_2(U)$ there are no remaining negative-energy waves and the driver can no longer absorb energy, and for $a < a_3(U)$ a pinch coincidence between two real modes (leading to divergent driver admittance) no longer occurs. As already mentioned, in typical flow conditions $a_1(U)$ is an exceedingly large number, while $a_{2,3}(U)$ are somewhat smaller but still very large. Finally, in §5 we indicate how the inclusion of plate dissipation modifies our results, and in parallel with Abrahams & Wickham (1994) for the flat plate we show how, for a very general set of parameter values, the system then becomes absolutely unstable at all flow speeds for $a > a_2(U)$.

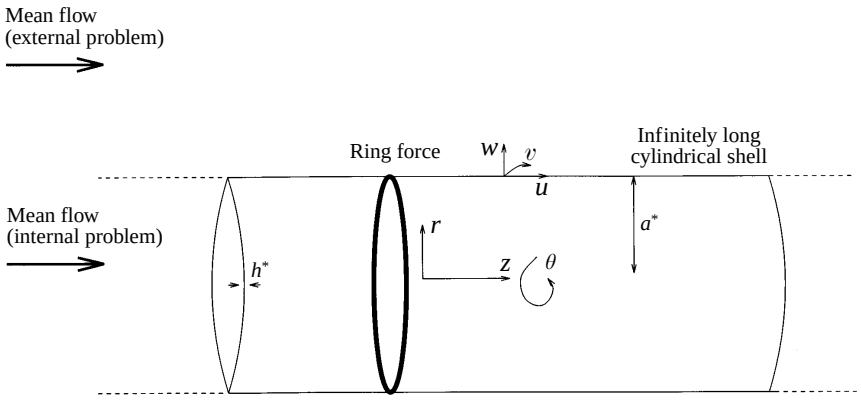

FIGURE 1. The cylindrical shell. The mean flow is aligned parallel to the cylinder axis and is located either (i) outside the cylinder, with a vacuum inside, or (ii) inside the cylinder with a vacuum outside.

2. Formulation and solution

2.1. *Governing equations*

We consider an infinitely long elastic cylinder, with a uniform circular cross-section of outer radius a^* and plate thickness h^* (in what follows the superfix * denotes dimensional quantities), and introduce plane polar coordinates (r^*, θ, z^*) with the cylinder axis lying along the z^*-axis – see figure 1. The cylinder is subjected to a localized ring force at $z^* = 0$ of the form $F^*(t^*)\exp(\mathrm{i}m\theta)\delta(z^*)$ in the outward normal direction, where m is an integer and t^* is the time. The force is switched on at the initial instant $t^* = 0$, so that $F^*(t^*) = 0$ for $t^* < 0$. Given the circular symmetry of the problem it follows that the azimuthal dependence of all flow quantities will be included in the multiplicative factor $\exp(\mathrm{i}m\theta)$, but clearly more complicated force distributions can be considered as a sum of these discrete modes. Inviscid incompressible fluid surrounds the cylinder, and in what follows we consider two possible scenarios: (i) the fluid lies outside the cylinder and possesses a steady mean speed U^* in the positive z^*-direction, with a vacuum inside the cylinder (this will be referred to as the *exterior* problem); (ii) the fluid lies inside the cylinder, again with uniform mean flow in the positive z^*-direction, with a vacuum outside the cylinder (this is the *interior* problem). The case in which fluid lies both inside and outside is an entirely straightforward generalization of these problems, and will not be considered further. It should be noted here that one feature omitted from our present study is the effect of gravity, which would clearly depend on the relative densities of the solid and of the fluids inside and outside the cylinder, as well as on the orientation of the cylinder. In the Appendix we note how gravitational effects are included in a simpler two-dimensional model.

The fluid and solid densities are ρ_0^* and ρ_s^* respectively, and the quantity c_p^* (see Junger & Feit 1986, equation 2.53) is given by

$$c_p^{*2} = \frac{E^*}{(1-\nu^2)\rho_s^*}, \tag{2.1}$$

with E^* and ν the Young's modulus and the Poisson ratio for the solid (note that the fluid sound speed is infinite, since the flow is incompressible). We now non-dimensionalize all lengths by h^*/ρ, time by $\sqrt{12}h^*/(c_p^*\rho^2)$ and pressures by $\rho_0^*\rho^2(c_p^*)^2/12$, where ρ is the fluid–solid density ratio ρ_0^*/ρ_s^*. The normalized ring force per unit

length is $F_0 = F_0^*/(\rho_s^* h^* c_p^{*2})$. We shall suppose that the cylindrical shell is thin, so that $h^*/a^* \ll 1$, and that the plate displacements are small, and the motion of the cylindrical shell under fluid loading is therefore described by Donnell's thin-shell equations. The axial, azimuthal and radial plate displacements are denoted $[u, v, w](z, t)\exp(\mathrm{i}m\theta)$ respectively, and from Junger & Feit (1986, p. 217) it follows that the thin-shell equations are

$$\frac{\partial^2 u}{\partial z^2} - \frac{(1-\nu)}{2a^2}m^2 u + \frac{\mathrm{i}(1+\nu)}{2a}m\frac{\partial v}{\partial z} + \frac{\nu}{a}\frac{\partial w}{\partial z} - \frac{\rho^2}{12}\frac{\partial^2 u}{\partial t^2} = 0, \tag{2.2a}$$

$$-\frac{m^2}{a^2}v + \frac{(1-\nu)}{2}\frac{\partial^2 v}{\partial z^2} + \frac{\mathrm{i}(1+\nu)}{2a}m\frac{\partial u}{\partial z} + \frac{\mathrm{i}m}{a^2}w - \frac{\rho^2}{12}\frac{\partial^2 v}{\partial t^2} = 0, \tag{2.2b}$$

$$a\nu\frac{\partial u}{\partial z} + \mathrm{i}mv + w + \frac{\rho^2}{12a^2}\left(a^4\frac{\partial^4 w}{\partial z^4} - 2a^2m^2\frac{\partial^2 w}{\partial z^2} + m^4 w\right) + \frac{a^2\rho^2}{12}\frac{\partial^2 w}{\partial t^2} = -\frac{a^2\rho^2}{12}[p(a,z,t)]_-^+ + F_0 a\delta(z), \tag{2.2c}$$

to be applied on $r = a$, where $a = a^*\rho/h^*$. Here $[p(a,z,t)]_-^+\exp(\mathrm{i}m\theta)$ is the jump in the fluid hydrodynamic pressure across the cylinder surface, and is equal to

$$\pm p(a\pm, z, t)\exp(\mathrm{i}m\theta)$$

for the external and internal problems respectively; its appearance in the third shell equation corresponds to the effects of fluid loading on the cylinder motion. The fluid pressure is obtained from the linearized unsteady Bernoulli equation in the form

$$p = -\left(\frac{\partial\phi}{\partial t} + U\frac{\partial\phi}{\partial z}\right), \tag{2.3}$$

where $U = U^*\sqrt{12}/(c_p^*\rho)$ is the non-dimensional mean-flow speed and $\phi(r,z,t)\exp(\mathrm{i}m\theta)$ is the fluid velocity potential. For irrotational flow this potential satisfies Laplace's equation

$$\nabla^2\phi = 0 \tag{2.4}$$

in $r > a$ (external) and $r < a$ (internal), which must be solved subject to the conditions of regularity at either $r = \infty$ or $r = 0$ respectively. In addition, we have the boundary condition of the continuity of normal velocity on the cylinder surface, which in the limit of small shell thickness and displacement considered here becomes

$$\frac{\partial w}{\partial t} + U\frac{\partial w}{\partial z} = \frac{\partial\phi}{\partial r} \quad \text{on} \quad r = a. \tag{2.5}$$

Finally, we demand that the solution is causal (i.e. unsteady flow variables are zero for $t < 0$), and equations (2.2)–(2.5) then specify the unique motion of the cylinder and the fluid. Our aim will be to determine this solution in the long-time limit $t \to \infty$, and this is described in the next subsection.

2.2. *Mathematical solution*

We begin by defining the Fourier transform in the axial coordinate z and time t, with for instance

$$\bar{w}(k,\omega) = \int_{-\infty}^{\infty}\int_{-\infty}^{\infty} w(z,t)\exp(\mathrm{i}\omega t - \mathrm{i}kz)\mathrm{d}z\mathrm{d}t. \tag{2.6}$$

Now transforming equations (2.2)–(2.5) and then completing a considerable amount of straightforward algebra, we can determine expressions for the three plate displace-

ments and the fluid velocity potential in terms of Fourier inversion integrals. For example, we find for the radial plate displacement

$$w(z,t) = -\frac{3}{\pi^2 a\rho^2}\int_C\int_{-\infty}^{\infty}\frac{\bar{F}_0(\omega)}{D(k,\omega;m)}\exp(-\mathrm{i}\omega t + \mathrm{i}kz)\mathrm{d}k\mathrm{d}\omega. \tag{2.7}$$

Here the spatial inversion (or k) contour is chosen to be the real k-axis, and in order to enforce causality the temporal inversion (or ω) contour C is chosen to be a straight line running parallel to the real ω-axis and lying above all singularities in the ω-plane. Note that $\bar{F}_0(\omega)$, the time-transform of the normalized driving force, is analytic in the upper half of the ω-plane, so that the condition on C corresponds to the requirement that it lies above all ω zeros of the dispersion function $D(k,\omega;m)$ for $-\infty < k < \infty$. The dispersion function is $D(k,\omega;m) = \mathscr{D}(k,\omega;m)/\Lambda(k,\omega;m)$, where

$$\mathscr{D}(k,\omega;m) = \left\{\Lambda(k,\omega,m)\left(-\frac{12}{\rho^2 a^2} - (k^2+\tilde{m}^2)^2 + \omega^2 - (\omega - Uk)^2\mathscr{F}(k;a)\right)\right.$$
$$\left. -\frac{\omega^2}{a^2}\left(\tilde{m}^2 + \nu^2 k^2\right) + \frac{6(1-\nu)}{a^2\rho^2}\left(k^4\nu^2 + 2\tilde{m}^2k^2 + \tilde{m}^4\right)\right\}, \tag{2.8a}$$

$$\Lambda(k,\omega;m) = \left[k^2 + \tilde{m}^2 - \frac{\rho^2\omega^2}{12}\right]\left[\frac{(1-\nu)}{2}(k^2+\tilde{m}^2) - \frac{\rho^2\omega^2}{12}\right] \tag{2.8b}$$

and $\tilde{m} = m/a$. The factor $\mathscr{F}(k;r)$ is given by

$$\mathscr{F}(k;r) = \frac{\mathrm{K}_m(r|k|)}{|k|\mathrm{K}'_m(r|k|)} \quad \text{for the external problem}$$
$$= -\frac{\mathrm{I}_m(r|k|)}{|k|\mathrm{I}'_m(r|k|)} \quad \text{for the internal problem,} \tag{2.9}$$

where $\mathrm{K}_m(z)$ and $\mathrm{I}_m(z)$ are modified Bessel functions of order m. The complex function $|k|$ arises from the transform of the bounded solutions of Laplace's equation, and is equal to k in the right half of the k-plane, and equal to $-k$ in the left half-plane. It is worth noting here that for all real values of k we have that $\mathscr{F}(k;r)$ is real and negative; for the external and internal problems this is best seen by use of the relations 9.6.24, p. 376 and 9.6.10, p. 375 respectively of Abramowitz & Stegun (1968).

We can see that the cylinder radius always occurs in the dimensionless group $a = a^*\rho_0/h^*\rho_s$, while the azimuthal mode number arises in the form m/a^2 apart from in the order of the special functions in $\mathscr{F}(k;m)$, and for a given choice of solid and fluid (in this paper usually steel in water) these two numbers completely specify the dispersion function. As we will see, the value of a has a crucial effect on the behaviour of our solution. Note that the dispersion relation for our system, $D(k,\omega;m) = 0$, is trivially equivalent to $\mathscr{D}(k,\omega;m) = 0$.

2.3. *Evaluation of the long-time limit*

The explicit evaluation of the integral in (2.7) for arbitrary t could be completed numerically, but in this paper we will be concerned with investigating the long-time limit ($t \to \infty$) of the solution analytically. In order to do this we apply the method first described by Briggs (1964) and Bers (1983), in which the long-time limit of the solution of our forced problem can be determined by studying the dispersion relation of the homogeneous unforced problem. The temporal contour C is deformed downwards onto the real ω-axis, causing the poles of the integrand in the k-plane, corresponding to the k-roots of the dispersion relation $D(k,\omega;m) = 0$, to move and to potentially

cross the real k-axis. In order to retain a causal solution, the k-contour must then be continuously deformed off the real axis so as to avoid any pole crossings. The reader is referred to Brazier-Smith & Scott (1984) for a particularly clear description of this method applied in fluid–structure interaction problems; it turns out that in our problem there are essentially four possible scenarios, which are described briefly below.

(*a*) The contour C can be deformed all the way down onto the real ω-axis without any poles crossing over the k-axis, so that the k-contour remains along the real axis, although possibly indented either above or below any poles which come to rest on the real k-axis. The question of whether such neutral modes are found either upstream or downstream of the driver at $z = 0$ then depends on which half of the k-plane the pole had originated from, or (in this case) entirely equivalently on the sign of the local group velocity $\partial\omega/\partial k$ on the real axis.

(*b*) A pole from the upper half of the k-plane crosses the real k-axis as C is lowered, necessitating a downward deformation of the k-contour. The pole is then picked up in $x > 0$, and corresponds to a convectively unstable wave downstream of the driver.

(*c*) A pole from the upper half-k-plane crosses the real k-axis as C is lowered in the ω-plane, but then turns round and moves back upwards so as to lie on the real k-axis once C has moved all the way down onto the real ω-axis (see figure 4). In such a situation the (neutral) mode will be located in $x > 0$, since it originated in the upper half of the k-plane, but its local group velocity on the axis is negative, incorrectly implying that the mode is to be found in $x < 0$. This behaviour results in an anomalous propagation effect, and this will be discussed fully in the context of our cylinder flow in §4.

(*d*) As the ω-contour C is lowered, poles in the k-plane coalesce, or pinch, from opposite sides of the k-axis, preventing further deformation of the k-contour. In this case it can be shown that the flow is absolutely unstable (again see Brazier-Smith & Scott 1984 for full details).

All four of the possible types of behaviour listed above are found by Crighton & Oswell (1991) for the flat plate with mean flow, and indeed they will also be found in our cylinder problem. However, we will see that plate curvature has a very marked effect on the range of parameter values over which these different regimes can exist, and in particular we will show how the more unexpected types of motion (namely (*c*), the anomalous propagation and (*d*), the absolute instability) actually only occur in our problem for exceedingly large, and it is claimed physically unrealistic, values of either the plate curvature parameter a or the flow speed U. This will be described in §3 and §4.

2.4. *Flat-plate solution*

Before going on to analyse the dispersion function for our cylinder, we briefly consider here the effect of taking the limit of very large cylinder radius. By sending $a \to \infty$ in (2.8), we find that

$$\mathscr{D}(k, \omega; m) \to \mathscr{D}_\infty(k, \omega) \equiv -k^4 + \omega^2 + \frac{(\omega - Uk)^2}{|k|}, \tag{2.10}$$

for both the external and the internal problems (because the ratio of the special functions in (2.9) approaches ∓ 1 respectively in their large-argument limits), and for any azimuthal mode number m (essentially because m occurs only as the order of the special functions or in the form m/a). The equation $D_\infty(k, \omega) = 0$ is exactly the dispersion function obtained by Brazier-Smith & Scott (1984) and Crighton & Oswell

(1991) for the problem of a fluid-loaded flat plate with mean flow. As might be expected, the effects of plate curvature therefore disappear in the limit $a \to \infty$, and our results will be seen to exactly match onto Crighton & Oswell's flat-plate results when a is very large – the question to be addressed here is how much plate curvature is required in order to produce a solution which differs significantly from Crighton & Oswell's result. The fact that the value of m does not feature in the dispersion relation in this limit is entirely understandable, since for a flat plate the normal displacement (i.e. w) is uncoupled from the transverse displacements (i.e. u, v), so that $\exp(\mathrm{i}m\theta)$ appears only as a purely unimportant transverse phase factor.

3. Absolutely unstable flow

3.1. *General case*

As described in (*d*) above, if two k-roots of $D(k, \omega; m) = 0$ pinch together from opposite halves of the k-plane as the ω-contour C is deformed downwards towards the real ω axis, then the deformation of C must be halted. Brazier-Smith & Scott (1984) describe the long-time behaviour of the solution in such a case: suppose the two k zeros coalesce at $k = k_p$ corresponding to $\omega = \omega_p$ with $\mathrm{Im}(\omega_p) > 0$, then as $t \to \infty$ the plate response (e.g. $w(z, t)$) will be dominated by a contribution at the complex frequency ω_p (so that $w(z, t) \propto \exp(-\mathrm{i}\omega_p t)$), and the response therefore grows exponentially in time for all z, so that the flow is absolutely unstable. It follows that in order to determine whether our forced problem is absolutely unstable or not, we simply need to look for suitable k pinch points in the unforced dispersion relation $D(k, \omega; m) = 0$. In practical terms, however, it is more straightforward to look for saddle points of D (i.e. points where $\partial\omega/\partial k = 0$), and provided that such a saddle point corresponds to a frequency with a positive imaginary part, and provided that the topology in the k-plane is such that the saddle is formed by coalescence of modes from opposite half-planes, then the saddle will indeed correspond to a point of absolute instability. Such a 'pinch' point can be found in the present problem, and by analogy with Crighton & Oswell (1991) it is to be expected that for this saddle we will find $\mathrm{Im}(\omega_p) > 0$ for $U > U_c(a, m)$, leading to absolute instability, while for $U \leqslant U_c$ we will have $\mathrm{Im}(\omega_p) \leqslant 0$ and the flow will be at worst convectively unstable. This indeed turns out to be the case.

Unlike the flat-plate problem, it is not possible to determine the exact absolute instability boundary for the cylinder in closed form, and we therefore proceed numerically. First, for a given value of U (say $U = 1$) and a very large value of a (in this case say $a = 1000$) the (absolutely unstable) saddle point was located in the k-plane by Newton iteration, using as a first guess the position of the saddle calculated from Crighton & Oswell's (1991) result. The value of a is then decreased in small increments, and the new location of the saddle recalculated, again using Newton iteration. In this way we can determine the value of a at which the imaginary part of the saddle frequency becomes zero, and our given value of U then corresponds to the absolute instability boundary $U_c(a, m)$ for this a. The whole process is repeated for a wide range of values of U, allowing the absolute instability boundary to be plotted as a function of a. At each stage care must be taken to verify that the saddle still corresponds to a genuine pinch, and that no other absolutely unstable saddles exist (this is best verified simply by inspection of contour maps of ω in the k-plane). In order to zero $\partial\omega/\partial k$ using Newton iteration it is necessary to calculate $\partial^2\omega/\partial k^2$, and care must be taken in calculating this second derivative accurately. It was found that

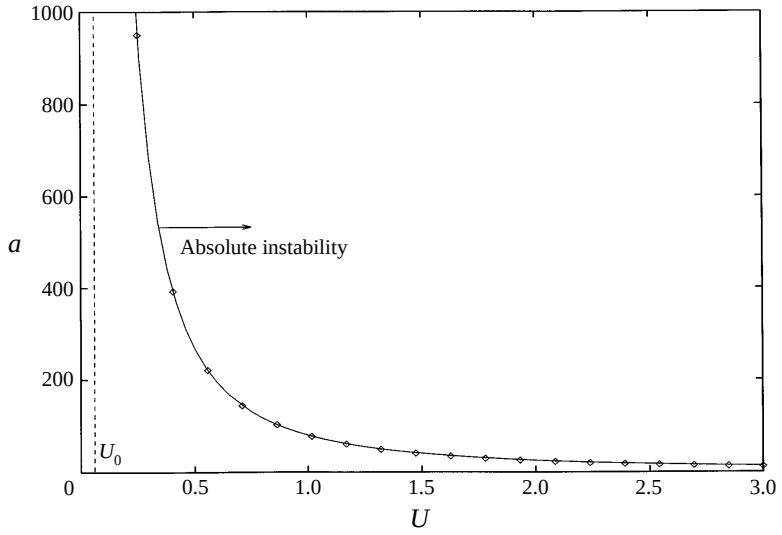

FIGURE 2. The absolute instability boundary. The value of flow speed U corresponding to the absolute instability boundary is plotted against curvature parameter a for the external problem with $m = 0$ (solid line) compared with the asymptotic result for small U (diamond symbols). The vertical dashed line represents the Crighton & Oswell absolute instability boundary $U = U_0$.

Cauchy's integral formula for the second derivative was particularly accurate and convenient, since it involves the evaluation of just ω (and not any of its derivatives) on a closed curve surrounding the point of interest in the k-plane.

Our numerical results for the absolute instability boundary of the external problem $U_c(a, m)$ with $m = 0$ are shown in figure 2. Unless otherwise stated, we consider throughout this paper the case of steel in water, so that $\rho_0 = 1000$ kg m^{-3}, $\rho_s = 7800$ kg m^{-3} (density ratio $\rho = 0.128$), $c_p^* = 5300$ m s^{-1} and the Poisson ratio is $\nu = 0.3$. As expected, the absolute instability boundary asymptotes to the Crighton & Oswell result of $U_0 \approx 0.074$ when $a = \infty$, but as a is reduced the critical value of U increases very rapidly indeed, with the consequence that absolute instability seems only to be possible for unachievably large values of either a or U. For instance, if we want the flow to be absolutely unstable for $U = 0.1$ (corresponding to $U^* = 19.6$ m s^{-1} for steel in water) then we require $a > 7700$ (corresponding to $a^*/h^* > 60000$). Conversely, in order to achieve absolute instability with say $a = 100$ (corresponding to $a^*/h^* = 780$) then we need $U > 0.87$ (i.e. $U^* > 171$ m s^{-1}), or with $a = 20$ ($a^*/h^* = 156$) we need $U > 2.2$ (i.e. $U^* > 435$ m s^{-1}). It should be noted that the absolute instability boundaries for the internal problem and for $m \neq 0$ are indistinguishable from that shown in figure 2, apart from at exceedingly large and unrealistic values of U (for which our original assumptions of incompressible flow are invalid anyway), and need not be considered further.

3.2. *Limit of small U*

As mentioned above, it has not proved possible to derive an analytical expression for the absolute instability boundary for general curvature parameter a and flow speed U. However, following Crighton & Oswell (1991) it is possible to make progress using the asymptotic limit $U \to 0$, and from figure 2 it is clear that in this limit the absolute instability boundary will correspond to $a \gg 1$. In practical underwater applications it seems that almost always $U \ll 1$, so that this limit is physically realistic.

The first step is to deduce the appropriate scalings of the axial wavenumber, k, and frequency, ω, when the flow is close to the absolute instability boundary (i.e. when the imaginary part of the pinch frequency is close to zero). Since absolute instability arises purely as an effect of the mean flow, we can suppose $\omega \sim Uk$, and further we know from Crighton & Oswell (1991) that the absolute instability boundary occurs when there is a balance between the fluid pressure term in the dispersion relation, which is proportional to $(\omega - Uk)^2\mathscr{F}(k;a)$, and the axial plate bending stiffness, which is proportional to k^4. By combining these two scalings and noting that $\mathscr{F}(k;a)$ is typically $O(1/|k|)$, we find that for small U the wavenumbers and frequency scale as $k = O(U^{2/3})$, $\omega = O(U^{5/3})$. Turning now to the question of the size of a, we find that the scaling $a = O(U^{-5/3})$ is a preferred limit, and substituting into (2.8) and expanding in powers of U, the dispersion relation becomes

$$k^4 - \frac{(\omega - Uk)^2}{|k|} - \omega^2 + \frac{12(1-\nu^2)}{\rho^2 a^2} + O(U^{11/3}) = 0. \tag{3.1}$$

Here, the first two terms are $O(U^{8/3})$ and the second two are $O(U^{10/3})$; the remaining terms in (2.8) occur at a higher order in U and are ignored – the largest such term occurs at $O(U^{11/3})$ and arises from the large-argument expansion of $\mathscr{F}(k;a)$. Note that since we are considering large values of a the azimuthal motion is again decoupled so that m does not feature in the asymptotic dispersion relation, and the only effect of curvature which survives is the fourth term in (3.1). This term corresponds to the contribution to the plate stiffness from the material stress in the azimuthal direction, and is of course absent for a flat plate. Interestingly, Dr A. D. Lucey (1996, personal communication) has pointed out that the dispersion relation (3.1) is equivalent to that of an infinite two-dimensional flat plate in mean flow, but with a spring foundation; for completeness, the equations of motion and the dispersion relation for such a system are included in the Appendix.

Absolute instability can arise when (3.1) possesses a double root in the k-plane for a given ω with $\mathrm{Im}(\omega) > 0$. For a polynomial dispersion relation of the form (3.1), Crighton & Oswell (1991) point out that marginal absolute instability occurs when this double root coincides with a third k-root of the dispersion relation to yield a triple root on the real k-axis (in Crighton & Oswell's notation, the absolute instability arises from the pinching of the modes $k^+_{1,3}$, and marginal absolute instability from the coalescence of these modes with k^+_2 – see figure 4). The condition for a triple root can easily be determined by differentiating (3.1) twice, and after some algebra we find that this triple root occurs at

$$k = \frac{U^{2/3}}{10^{1/3}}, \quad \omega = \frac{U^{5/3}3^{1/2}}{2^{1/3}5^{5/6}}, \tag{3.2}$$

provided that U satisfies the implicit relation

$$a^2 = +\frac{(1-\nu^2)5^{5/3}2^{8/3}}{\rho^2 U^{8/3}[U^{2/3} - U_0^{2/3}]}, \tag{3.3}$$

where

$$U_0 = \frac{5^{5/4}2^{1/2}}{3^{3/4}}\left[2 - \frac{15^{1/2}}{2}\right]^{3/2} \approx 0.074 \tag{3.4}$$

is the value of flow speed corresponding to Crighton & Oswell's absolute instability

boundary for a flat plate (for steel in water $U_0^* = 14.5$ m s^{-1}). It follows that for $U \ll 1$ our cylinder problem is absolutely unstable for values of U greater than the single positive real solution of (3.3), and is at worst convectively unstable for values of U below this critical value. Note that as $a \to \infty$ in (3.3) our value for U at the absolute instability boundary agrees exactly with that found by Crighton & Oswell (1991) in the flat-plate case, while for finite, but large, values of a the bounding value of U is greater than U_0, in agreement with the numerical solution in §3.1. In fact, the boundary described by (3.3) is plotted in figure 2, and is seen to be indistinguishable from the absolute instability boundary calculated numerically from the full dispersion relation. We also note, by putting the dimensions back into (3.3), that for a given flow speed U^* the minimum value of a^*/h^* needed for absolute instability is proportional to ρ_s^*/ρ_0^*. As we saw in §3.1, these values of a^*/h^* are very large indeed for steel in water, but for steel in air ($\rho_0 \approx 1.3$ kg m^{-3}) it follows that the corresponding minimum of a^*/h^* is some 745 times larger still! The form of equation (3.3) confirms that $a = O(U^{-5/3})$ is indeed a preferred limit for the analysis of the absolute instability of our cylinder. If $a > O(U^{-5/3})$ then the curvature has no effect on the absolute instability boundary, which is then given exactly by the flat-plate result $U = U_0$. If $a < O(U^{-5/3})$ then the scalings described here can no longer predict the absolute instability boundary, which must instead be determined numerically as in the previous subsection.

4. Convectively unstable and stable flow

In the previous section we showed that our flow was absolutely unstable if the non-dimensional mean flow speed U is larger than a critical value $U_c(a, m)$. In this section we shall suppose that $U < U_c(a, m)$ so that the flow can be at worst convectively unstable, and so that the Briggs–Bers method can potentially exhibit the possible types of behaviour (*a*), (*b*) and (*c*) described in §2.3. This means that in determining the long-time limit of our solution the temporal inversion contour C can be deformed all the way down onto the real ω-axis, and in what follows we are therefore able to consider real frequencies.

4.1. *Behaviour of dispersion curves*

Here we consider dispersion curves $\omega = \omega(k)$, where $D(k, \omega; m) = 0$ with ω real – note that the dispersion relation is invariant under $k \to -k, \omega \to -\omega$, so that we need consider only $k > 0$. In figure 3 we plot the dispersion curves for $U = 0.05$ (the test case used by Crighton & Oswell 1991, corresponding for steel in water to $U^* = 9.8$ m s^{-1}) with $m = 0$ and for four different values of the curvature parameter a. In this axisymmetric case the dispersion relation reduces to a quartic in ω, but two of the roots approximate (for large a) to the compressional waves $\omega = \mp(12^{1/2}/\rho)k$, which appear to exhibit no unusual features and are therefore omitted from further consideration. In figure 3(*a*) we have the very large value of $a = 25000$ (for steel in water corresponding to $a^*/h^* = 1.95 \times 10^5$), and we can see that the dispersion diagram has three distinct regions. For $k < k_a$ and for $k > k_b$ the two ω-roots are real and the system is stable, while for $k_a < k < k_b$ the two ω-roots are complex. By applying the Briggs–Bers method one can demonstrate that these complex poles exhibit behaviour (*b*) of §2.3, so that the flow is convectively unstable. (Note also that for $\omega > \omega_p$ there exist additional complex k-roots, but these correspond to waves which decay away from the driver, and need not be considered further.) At $k = k_{a,b}$ (frequencies $\omega_{a,b}$) the group velocity $\partial\omega/\partial k$ is infinite, corresponding to branch points

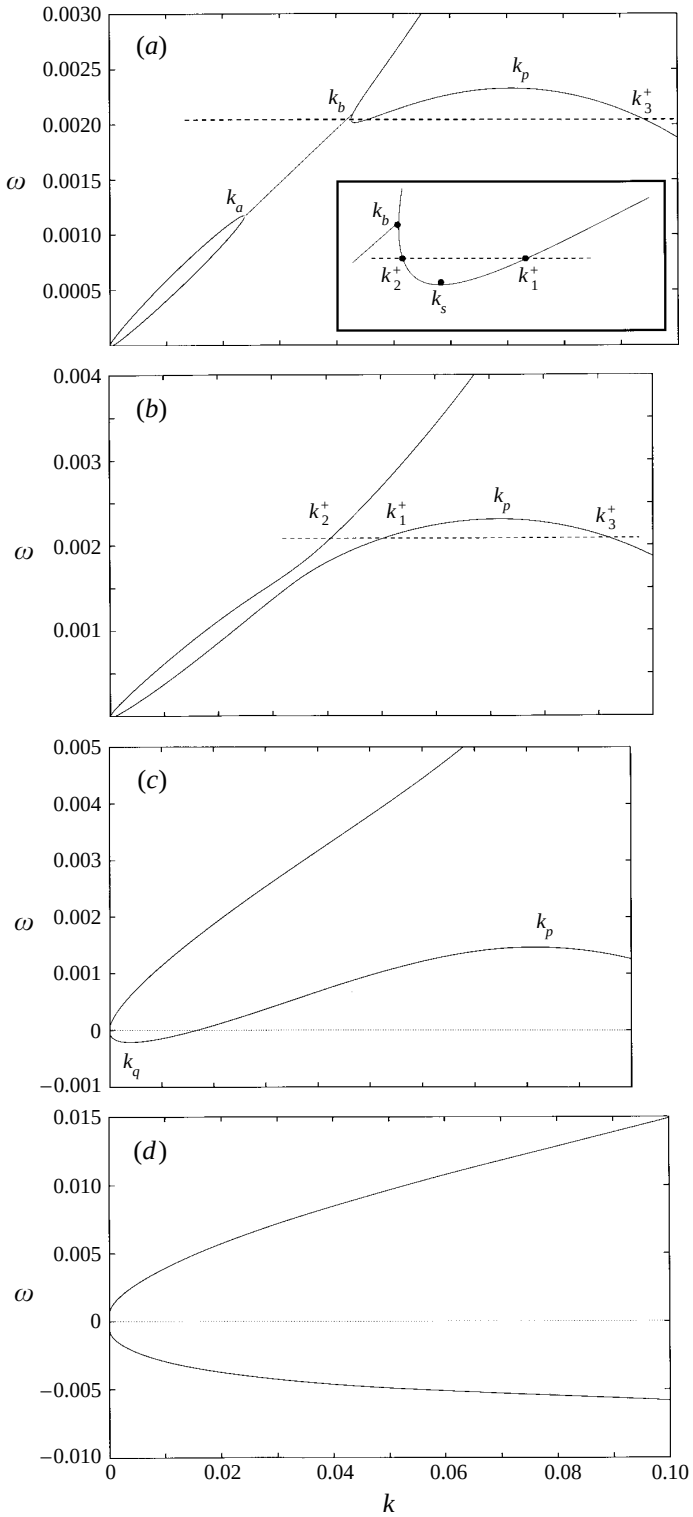

FIGURE 3. For caption see facing page.

of the dispersion function, while at $k = k_{s,p}$ (Crighton & Oswell's notation) the group velocity is zero. It is worth noting here that for a flat plate ($a = \infty$) the dispersion curve looks exactly like the one shown in figure 3(*a*), except that the real branch to the left of the point $k = k_a$ is missing so that the flow is then convectively unstable for all $k < k_b$. In figure 3(*b*) and 3(*c*) we have smaller, but still large, values of a and it can be seen that the region of convective instability has now disappeared, so that the system is stable for all k (again spatially decaying modes exist for $\omega > \omega_p$). The group velocity now vanishes at two points on the lower branch: at the point $k = k_p$ as before, and at the point $k = k_q$ (which in figure 3*a*, *b* is exceedingly close to $k = 0$, but which moves away from $k = 0$ as a is decreased). Finally, for a much smaller value of $a = 500$ (corresponding to the still large value of $a^*/h^* = 3900$) in figure 3(*d*), the system is stable for all k and the group velocity is never zero. We can therefore conclude that as a is reduced from infinity the form of the dispersion curves changes as shown in figure 3; by considering the full dispersion relation (2.8), it was found numerically that for the conditions in figure 3 the region of convective instability vanishes at approximately $a = 21\,370$ (i.e. the transition from figure 3*a* to figure 3*b*), while the points of zero group velocity coalesce and then disappear at $a = 1165$ (i.e. the transition from figure 3*c* to figure 3*d*).

It is possible to investigate this change in behaviour using asymptotic analysis in the limit of small U. Following Crighton & Oswell (1991), it can be seen from figure 3 that k and ω are both small, and since we are interested in mean-flow effects we again suppose that $\omega = O(Uk)$. We will see that in the preferred limits for describing the above behaviour we have $ak \gg 1$, so that using the large-argument expansions of the various special function we can replace $\mathscr{F}(k;a)$ in (2.8) by $-1/|k|$. Moreover, provided $m = O(1)$ the terms in (2.8) involving $\tilde{m}$ can be set to zero, and it therefore follows that our dispersion relation $D(k, \omega; m) = 0$ can be simplified to

$$\omega^2(k+1) - 2Uk\omega - \frac{12(1-\nu^2)}{\rho^2 a^2}k - k^5 + U^2k^2 = 0, \tag{4.1}$$

which is identical to the approximation specified in (3.1). We now calculate the group velocity from this dispersion relation in the form

$$\frac{\partial\omega}{\partial k} = \frac{2UA_1^{1/2} \pm A_2}{2(k+1)^2 A_1^{1/2}}, \tag{4.2}$$

where

$$\left.\begin{aligned} A_1 &= k^6 + k^5 - U^2k^3 + \frac{12(1-\nu^2)}{\rho^2 a^2}k(k+1), \\ A_2 &= 4k^6 + 9k^5 + 5k^4 - U^2k^3 - 3U^2k^2 + \frac{12(1-\nu^2)}{\rho^2 a^2}(k+1). \end{aligned}\right\} \tag{4.3}$$

If we set $a = \infty$, then (4.2) reduces exactly to the flat-plate result (Crighton & Oswell

FIGURE 3. The dispersion curves for the external problem with the full dispersion relation (2.8) with $U = 0.05$, $m = 0$ and with (*a*) $a = 25000$, (*b*) $a = 20000$, (*c*) $a = 4000$, (*d*) $a = 500$. In (*a*) and (*b*) the broken lines denote the frequency $\omega = 0.002016$ used in figure 4. The material parameters used here correspond to steel in water, and are described in §3.1. In (*a*) the dotted line joining k_a and k_b corresponds to the real part of the convectively unstable mode.

1991, equation 5.10). We also note here that in limit of small U

$$\frac{\partial D}{\partial \omega} = \pm \frac{A_1^{1/2}}{k^2 - \frac{1}{12}\rho^2\omega^2} \tag{4.4}$$

for ω, k satisfying the dispersion relation, where $\pm$ denote the upper and lower branches of the dispersion curve.

At the branch points $k = k_{a,b}$ the group velocity is infinite, and according to Crighton & Oswell's analysis $k_b = O(U)$. In order to determine $k_{a,b}$ we therefore set $k = O(U)$ and adopt the preferred scaling on a, which turns out to be $a = O(U^{-2})$. For infinite group velocity (4.2) implies we need $A_1 = 0$ for some k, and substituting in the above scalings results in a quadratic in k^2. The condition that the branch points $k = k_{a,b}$ exist for real k is then equivalent to the requirement that this quadratic possesses real roots, so that the necessary and sufficient condition for the branch points to occur for real k is that

$$a > a_1(U) = \left[\frac{48(1-v^2)}{\rho^2 U^4}\right]^{1/2}. \tag{4.5}$$

Our system is therefore convectively unstable for $a > a_1(U)$ and stable for $a < a_1(\mathrm{U})$. As might be expected, the length of the convectively unstable region on the k-axis is extended by increasing either the mean-flow speed or the fluid–solid density ratio. For the parameters considered in figure 3, equation (4.5) yields $a_1 = 20\,620$, which agrees with the result of $a_1 = 21\,370$ found numerically from the full dispersion relation with an error of only 3%.

The existence of the points of zero group velocity at $k = k_{s,p,q}$ can be analysed in much the same way as above. It can be shown from (4.2) that the values of k where $\partial\omega/\partial k = 0$ satisfy

$$U^2 = \frac{F(k^3+3k^2)+2G}{(k^3+3k^2)^2+4k^3}\left\{1 \pm \left(1 - \frac{F^2[(k^3+3k^2)^2+4k^3]}{[F(k^3+3k^2)+2G]^2}\right)^{1/2}\right\}, \tag{4.6}$$

where

$$\left.\begin{aligned} F &\equiv \frac{12(1-v^2)}{\rho^2 a^2}(k+1) + 4k^6 + 9k^5 + 5k^4, \\ G &\equiv A_1 + U^2 k^3. \end{aligned}\right\} \tag{4.7}$$

For the point $k = k_s$ we again choose $k = O(U)$, and the preferred limit of a again turns out to be $a = O(U^{-2})$. By substituting these scalings into the larger root in (4.6) and then expanding in powers of U, it is easy to show that (4.6) reduces to

$$U^2 = k^2 + \frac{12(1-v^2)}{\rho^2 U^4 k^2}. \tag{4.8}$$

The condition for the existence of the turning point at $k = k_s$ is then equivalent to the condition that this equation possesses a real k-root, and this is exactly the condition (4.5). Alternatively, for the turning points at $k = k_{p,q}$ we take the scaling $k = O(U^{2/3})$ (i.e. the same as in the absolute instability case), and it turns out that the preferred limit of a is now $a = O(U^{-4/3})$. Substituting these scalings into (4.6) and expanding in powers of U, we now find that at these turning points we have

$$U = \frac{5k^4 + 12(1-v^2)/\rho^2 a^2}{2\left(k^5 + [12(1-v^2)/\rho^2 a^2]k\right)^{1/2}}, \tag{4.9}$$

which for $a = \infty$ agrees exactly with the Crighton & Oswell result of $k = (4U^2/25)^{1/3}$. The existence of the turning points for real $k_{p,q}$ then depends on equation (4.9) possessing two real positive roots, and this reduces to the condition of the form $a > a_3(U)$ (at $a = a_3(U)$ the two real positive roots coalesce to yield a single real point of zero group velocity, while for $a < a_3(U)$ no positive real roots of (4.9) exist). It has not proved possible to find $a_3(U)$ explicitly, but numerical calculations are very straightforward: for the parameter values used in figure 3 we find from (4.9) that $a_3 = 1176$, which agrees with the value of $a_3 = 1165$ determined using the full dispersion relation (2.8) with an error of only 1%. Also, we find that a_3 decreases monotonically with increasing U and increasing ρ. It is worth noting here that the 'pinch' points $k = k_{p,q}$ are significant since they possess zero group velocity, and the corresponding modes would not tend to propagate away from their point of initial excitation. These modes would therefore tend to be a feature of the response at that point even at late times.

We note that the turning point $k = k_p$ moves to progressively lower frequency $\omega = \omega_p$ as a is reduced towards a_3 (see figure 3*a*, *b*). We will see later that the condition $\omega_p = 0$ is particularly significant, and it is again possible to use the large-a asymptotics to estimate when this happens. By setting $\omega, \partial\omega/\partial k = 0$ in both equation (4.1) and its k-derivative, we find that $\omega_p \geqslant 0$ when $a \geqslant a_2(U)$, where

$$a_2(U) = \frac{2^{7/3}(1 - v^2)^{1/2}}{\rho U^{4/3}}. \tag{4.10}$$

For the conditions used in figure 3 we calculate $a_2 = 2036$, which agrees exceedingly well with the value of $a_2 = 2040$ found by examining the full dispersion relation numerically.

Finally, it is of some interest to consider the behaviour of the dispersion curves for small k, particularly since in our problem real modes are present right down to zero wavenumber, in contrast to the flat-plate problem in which modes with $k < k_b$ are complex. For small k we see from (4.1) that

$$\omega = Uk \pm \left[\frac{12(1 - v^2)k}{\rho^2 a^2}\right]^{1/2} + O(k^{3/2}). \tag{4.11}$$

These two branches of course correspond to the two branches seen in figure 3 close to $k = 0$, and to this order in k are equally spaced about the uniform-flow curve $\omega = Uk$. When a is very large indeed (in fact $a > O(U^{-4/3})$), differentiation of (4.11) confirms the presence of the point of zero group velocity k_q very close to the origin – in fact, this value of k_q exactly agrees with that found by taking the small-k limit in (4.9). Moreover, it can be seen that the group velocity determined from (4.1) becomes infinite at $k = 0$.

4.2. *Spatial location of modes*

In order to determine the spatial location of the neutral modes rigorously (i.e. either upstream or downstream of the driver) we must use the Briggs–Bers method as outlined in §2, whereby $\mathrm{Im}(\omega)$ is decreased from some large positive value towards zero. For the values of a used in figure (3*a*, *b*) we plot the loci of the various roots for a single frequency satisfying $\omega_b < \omega < \omega_s$ in figure 4 (this frequency is marked by the broken lines in figure 3*a*, *b*). The modes denoted $k^+_{1,3}$ (Crighton & Oswell's notation) originate in the upper and lower halves of the complex k-plane for large $\mathrm{Im}(\omega)$, and move monotonically onto the real axis as $\mathrm{Im}(\omega)$ is reduced to zero;

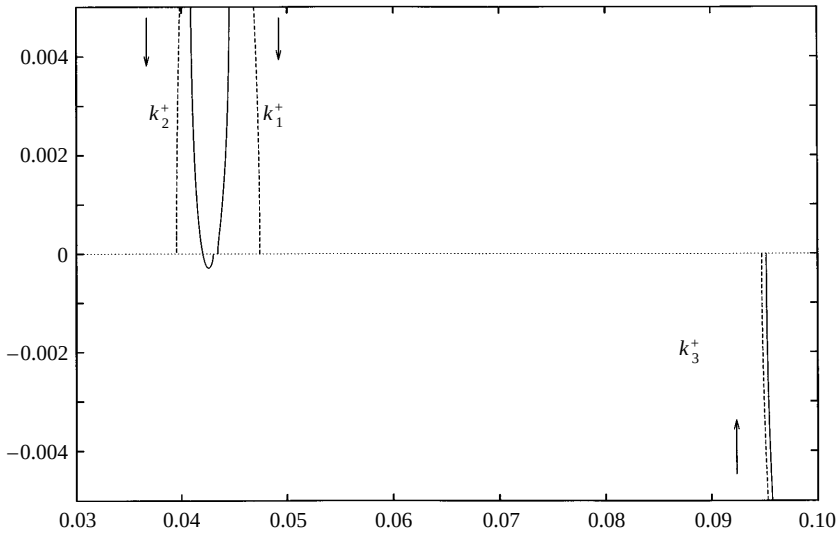

FIGURE 4. The loci of certain k modes in the complex k-plane as $\mathrm{Im}(\omega)$ is reduced to zero with $\mathrm{Re}(\omega) = 0.002016$, with conditions as in figure 3 and with $a = 25000$ (i.e. $a > a_1$ solid lines) and $a = 20000$ (i.e. $a < a_1$ dotted lines). The arrows indicate the direction of motion as ω approaches the real axis.

$k_{1,3}^+$ are therefore found in $x > 0$ and $x < 0$, and with group velocities pointing downstream and upstream, respectively for both values of a. On the other hand, the mode k_2^+ originates in the upper half-plane, and for $a > a_1$ it then moves into the lower half-plane before coming to lie on the real axis from below once $\mathrm{Im}(\omega) = 0$ (i.e. behaviour c) of §2.3). Hence, the k inversion contour must be deformed below $k = k_2^+$, and the mode is found in $x > 0$ but with its group velocity pointing (anomalously) upstream. This exactly matches the behaviour found by Crighton & Oswell for the flat-plate problem (cf. their figure 7), who show that $k_2^+(\omega)$ exhibits this anomalous behaviour for any frequency in the anomalous range $\omega_s < \omega < \omega_b$. Alternatively, for $a < a_1$ we see in figure 4 that the mode k_2^+ moves straight onto the real k-axis without first entering the lower half-plane, so that it is again found in $x > 0$ but this time with its group velocity pointing (conventionally) downstream.

An alternative method of determining the spatial location of neutral modes is to apply Lighthill's (1960) local group velocity criterion: for a neutral mode $k(\omega)$ with ω real, fictitious damping is introduced as an imaginary part of the frequency, so that $k(\omega) \to k(\omega + \mathrm{i}\epsilon)$ with ϵ small and positive. The displacement of the mode off the real k-axis, and hence the required deformation of the inversion contour and consequent spatial location of the mode, then depends on the local group velocity $\partial\omega/\partial k$. Lighthill's criterion states that for systems where the driver is the only source of energy, the local group velocity of the mode must be directed away from the driver. When applied to the modes $k_{1,3}^+$ this criterion is in agreement with the conclusions reached above using the Briggs–Bers method: $k_{1,3}^+$ have positive (and is found downstream) and negative (and is found upstream) local group velocities for $\mathrm{Im}(\omega) = 0$ respectively. However, the Lighthill criterion is at variance with the result for the mode k_2^+ for $a > a_1$, which has a negative local group velocity on the axis but which is found downstream of the driver. The reason for this discrepancy is of course that in our problem both the driver and the mean flow are sources of energy so that Lighthill's criterion is not necessarily applicable, and as is made clear in §4.4

energy can move both into and out of the system through the driver. Crighton & Oswell therefore emphasize that in the presence of mean flow the spatial location of the modes can only be reliably determined by consideration of the global behaviour of the k zeros of the dispersion relation in the whole complex plane.

The highly anomalous behaviour of the mode $k_2^+(\omega)$ in $\omega_s < \omega < \omega_b$ is perhaps the most striking and unexpected feature of Crighton & Oswell's analysis, and our aim here is to identify how this is modified by plate curvature. As seen in figure 4 the anomalous behaviour is certainly observed in our cylinder problem for the very large value of a used in figure 3(a), but not for the smaller (but still large) value used in figure 3(b). By plotting a whole series of graphs of the form shown in figure 4, it turns out that the anomalous behaviour is intimately connected with the existence of the branch point $k = k_b$. In fact, for $a < a_1(U)$ (for which no real branch points exist) the anomalous behaviour could not be found for any ω and a, so that in such cases the spatial location of the neutral modes could be correctly predicted using Lighthill's local group velocity criterion in an entirely obvious way. Also, it is worth emphasizing here that even for $a > a_1(U)$ no anomalous propagation behaviour was found for modes lying on the lower-wavenumber loop joining k_a to the origin (see figure 3a). As has already been noted, a_1 is an exceedingly large number, and this suggests that even a very small amount of plate curvature will be enough to eliminate Crighton & Oswell's anomalous propagation effect. For instance, for 2 cm thick steel plate in water with the mean flow speed 9.8 m s^{-1} (as in figures 3 and 4), the plate radius of curvature would have to be in excess of 3.3 km in order to observe the Crighton & Oswell anomalous propagation! Since such a large radius of curvature is quite unattainable in a practical engineering situation, it seems that the Lighthill local group velocity criterion is entirely applicable in practice to our problem.

4.3. *Energy considerations*

Benjamin (1963) has classified the neutral waves in compliant-surface problems according to their energy, E^*, defined to be the work done by an external force in creating the given steady-state wave from rest at $t = -\infty$ (or, more precisely, the increase in wall strain and kinetic energy minus the work done by the hydrodynamic forces on the wall in establishing the particular disturbance). Type A, or negative-energy, waves have $E^* < 0$, and their generation results in a decrease in the energy of the system relative to the quiescent state; negative energy waves are destabilized by damping effects, which act to reduce the wave energy and hence make E^* more negative. Type B, or positive-energy, waves have $E^* > 0$; their generation leads to an increase in the energy of the system and they are stabilized by damping. Cairns (1979) has derived an expression for E^* in terms of the system dispersion relation. Following his method, we consider a wave for which $w = A(T)\exp(\mathrm{i}k_0 z - \mathrm{i}\omega_0 t)$, where $A(T)$ is the wave amplitude which is a function of the slow time T over which the wave is built up from rest. Substituting this, and similar expressions for the transverse displacements, into the shell equations (2.2) yields an expression for the external force, $F_0(T)\exp(\mathrm{i}k_0 z - \mathrm{i}\omega_0 t)$, required to generate the wave, from which it can be shown that the normalized wave energy is

$$E \propto \omega_0 \frac{\partial D}{\partial \omega}|A|^2, \tag{4.12}$$

with the derivative of D evaluated at k_0, ω_0. It therefore follows that the sign of E is given exactly by the sign of $\omega_0 \partial D/\partial\omega$.

For the dispersion curves given in figure 3 it is an easy matter to verify numerically,

and in the limit of small U to prove analytically (using (4.4) and noting that $\omega \ll k$), that on the lower branches $\partial D/\partial\omega < 0$ and on the upper branches $\partial D/\partial\omega > 0$ (so in particular in figure 3(a) the lower branch includes the branch starting at the branch point $k = k_b$ and running through the points $k = k_{s,p}$). In figure 3 the waves on the lower branches with positive ω therefore correspond to negative-energy waves, and on the upper branches to positive-energy waves. In figure 3(d) note how both branches shown correspond to positive-energy waves, since $\omega < 0$ on the lower branch. We are therefore able to identify a critical value of a below which there are no negative-energy waves present in our system, and this critical condition must correspond to the turning point $k = k_p$ occurring at $\omega_p = 0$, so that no portion of the lower branch of the dispersion curve lies in $\omega > 0$. As shown at the end of §4.1, the condition for our system to possess negative-energy waves therefore corresponds to the requirement that $a > a_2(U)$, with $a_2(U)$ given by (4.10). Again considering 2 cm thick steel in water with $U = 0.05$, we find that we need a^* larger than 318 m in order to get negative-energy waves, which although considerably less than the corresponding value of a_1, also seems rather larger than might be found in most applications.

4.4. *Driver admittance*

It will prove illuminating to investigate the direction in which energy is flowing between the plate and the mean flow, and the simplest way to do this is to investigate the rate of working of the ring-force driver at $z = 0$. We consider single-frequency forcing (strictly the long-time limit of the start-up problem described in §2) with ring force $F_0 \exp(-\mathrm{i}\omega t)\delta(z)$, and the driver admittance $A_0(\omega)$ is then defined to be the ratio of the cylinder radial velocity at $z = 0$ to the amplitude of the forcing, so that $-\mathrm{i}\omega w(0) = A_0(\omega)F_0$. From equation (2.7) it is easy to show that

$$A_0(\omega) = \frac{6\mathrm{i}\omega}{\pi a\rho^2}\int_{-\infty}^{\infty}\frac{\mathrm{d}k}{D(k,\omega;m)}, \tag{4.13}$$

where the integration contour is the real k-axis indented above or below the k zeros of $D(k,\omega;m)$ in the way prescribed by the Briggs–Bers method described in §2.3. Note that the turning point $k = k_p$ is formed by the coalescence of the modes k_1^+ and k_3^+ from opposite sides of the k-axis, in which case it is not possible to deform the contour in (4.13) so as to avoid the singularity at $k = k_p$. Similarly, it appears that the turning point $k = k_q$ in figure 3(c) is also formed by modes pinching together from opposite sides of the real axis (the turning point at $k = k_s$ in figure 3(a) is formed by the merging of k_1^+ and k_2^+ from above the real axis and is not a pinch point); this means that $A_0(\omega)$ diverges whenever the turning points at $\omega_{p,q}$ exist. The rate of working of the ring force, integrated over all θ, can then be calculated as $\pi\mathrm{Re}(A_0)|F_0|^2$, from which it can be seen that the direction of power transfer through the driver depends on the sign of $\mathrm{Re}(A_0)$: if $\mathrm{Re}(A_0) > 0$ then the driver injects energy into the system, but if $\mathrm{Re}(A_0) < 0$ then the driver must absorb energy from the system.

In order to calculate $\mathrm{Re}(A_0)$ one only needs to consider contributions from poles which either lie on, or in the convectively unstable case $a > a_1(U)$ have crossed over, the real k-axis, which of course corresponds to the far-field action of the driver (the near-field action correspond to the Cauchy principal-value contributions to (4.13), which only feature in $\mathrm{Im}(A_0)$). In figure 5 we plot $\mathrm{Re}(A_0)$ against ω for two values of a. In figure 5(a) we have $a_2(U) < a < a_1(U)$, and note how $\mathrm{Re}(A_0)$ can take values of either sign, with infinities at the two pinch points $\omega = \omega_{p,q}$, while in figure 5(b) we have $a < a_3(U)$ and $\mathrm{Re}(A_0)$ is everywhere positive and finite.

The fact that $\mathrm{Re}(A_0)$ can be negative, corresponding to absorption of energy by the

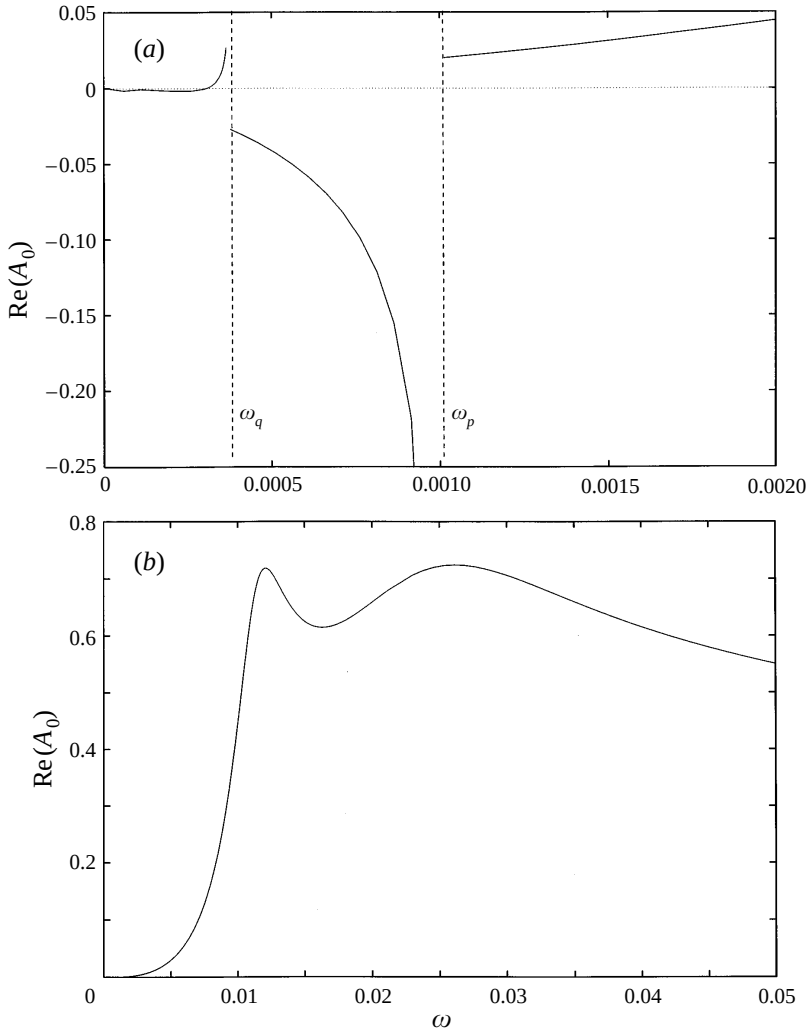

FIGURE 5. Plots of the real part of the driver admittance against frequency for the external problem. We have (*a*) $a = 4000$ ($a > a_2$) and (*b*) $a = 500$ ($a < a_3$), with other conditions as in figure 3.

driver from the mean flow, is linked to the presence of negative-energy waves. The energy flux in the positive x-direction associated with a neutral mode is simply $J = E\partial\omega/\partial k$. In figure 3(*a*) for the frequency $\omega_s < \omega < \omega_b$, the negative-energy modes $k^+_{1,3}$ have $J < 0$ and $J > 0$, and are located in $x > 0$ and $x < 0$, respectively and therefore contribute to the energy absorption by the driver. Crighton & Oswell (1991) clearly explain that the presence of these two negative-energy waves leads to $\mathrm{Re}(A_0) < 0$ for ω in this anomalous frequency range. (Interestingly, the negative-energy anomalous mode k^+_2 has $J > 0$ and is found in $x > 0$ and therefore actually contributes to the energy emission by the driver, but apparently not sufficiently to counteract the effect of the other two modes.) In our cylinder problem we have already shown that provided $a < a_1(U)$ then the sign of the local group velocity of a neutral mode correctly indicates its spatial location, from which it follows that any negative-energy waves will transport energy towards the driver (i.e. like modes $k^+_{1,3}$ above). Hence, as long as negative-

energy waves exist in our system it follows that there is potentially a net absorption of energy by the driver, and hence that $\mathrm{Re}(A_0) < 0$, for some range of ω. For $a > a_2(U)$ we can therefore have $\mathrm{Re}(A_0) < 0$, but for $a < a_2(U)$ there are no negative-energy waves and hence $\mathrm{Re}(A_0)$ must always be positive – this is fully confirmed in figure 5.

For figure 5(*a*) in the range $0 < \omega < \omega_q$ there exist both positive-energy waves (from the upper branch, and from the lower branch for negative k in figure 3*c*) and negative-energy waves (on the lower branch for positive k), so that as can be seen the admittance can take both positive and negative values depending on the relative magnitudes of these terms. As is clear in figure 5(*a*), the admittance approaches zero at small ω, but in fact it turns out to be rather difficult to resolve its precise behaviour numerically, due to the very close proximity of several roots of the dispersion relation. This difficulty could be addressed by use of the sort of asymptotic analysis for small ω carried out in §3 of Crighton & Oswell (1991), but this only seems tractable if one also uses $a \gg 1$ and $U \ll 1$ so as to simplify the dispersion relation. However, since the main purpose of this subsection is to verify the conclusions about the existence of negative-energy waves made earlier, we will not pursue this point further in the present paper. It suffices to say that the value of $\mathrm{Re}A_0$ appears to be insignificant for small values of ω in this range. Also, the distinct maximum on the curve shown in figure 5(*b*) presumably arises as the result of a balance between the contributions to the admittance by the various positive-energy waves, but does not seem to the author to admit any obvious physical interpretation.

5. The effects of dissipation

So far we have supposed that dissipation has been completely absent from our system. However, as has been explained by Cairns (1979), the effects of the inclusion of dissipation (for instance, by supposing that suitable plate parameters possess an imaginary, dissipative component) can be inferred from the sign of the wave energy: positive-energy waves are stabilized by dissipation, and negative-energy waves are destabilized. In this section we extend that argument by considering specifically the real pinch point at $k = k_p$, which as described in the previous section exists for $a > a_3$ and for $U < U_c(a, m)$ (for $U > U_c(a, m)$ the pinch point $k = k_p$ is complex and leads to absolute instability). We note that an exactly comparable analysis has been completed by Abrahams & Wickham (1994) for the fluid-loaded flat plate (i.e. $a = \infty$).

Consider first a general system in which the inclusion of a small amount of dissipation yields the dispersion relation

$$D(k, \omega) = -\mathrm{i}\epsilon V(k, \omega), \tag{5.1}$$

where $\epsilon \ll 1$ is a dimensionless measure of the magnitude of the dissipation, and $D(k, \omega) = 0$ is the dissipationless dispersion relation. Since the point $k = k_p$ is a pinch point, it follows that $D(k_p, \omega_p) = \partial D(k_p, \omega_p)/\partial k = 0$, and if we expand (5.1) in a Taylor series about the pinch point and then differentiate this expansion with respect to k, we find

$$\frac{\partial \omega}{\partial k}\left[D_\omega + (\omega - \omega_p)D_{\omega\omega} + (k - k_p)D_{k\omega}\right] + (k - k_p)D_{kk} + (\omega - \omega_p)D_{k\omega} + \ldots = -\mathrm{i}\epsilon\frac{\partial V}{\partial k} + \ldots, \tag{5.2}$$

where all the derivatives of D and V are evaluated at $k = k_p, \omega = \omega_p$ and the suffices here denote partial differentiation. We now look for a saddle point of the

full dispersion relation (5.1) by setting $\partial\omega/\partial k = 0$ in (5.2). If we suppose that this saddle point lies a small distance from the dissipationless pinch point, so that $|k - k_p|, |\omega - \omega_p| = O(\epsilon)$, then by expanding both (5.2) and the Taylor expansion of (5.1) in powers of ϵ we find an expression for the location of the saddle to $O(\epsilon)$ in the form

$$\left.\begin{aligned} \frac{\omega - \omega_p}{\omega_p} &= -\mathrm{i}\epsilon\left[\frac{V}{\omega D_\omega}\right]_{k=k_p,\omega=\omega_p}, \\ k - k_p &= \mathrm{i}\epsilon\left[\frac{V}{D_{kk}}\left(\frac{D_{k\omega}}{D_\omega} - \frac{V_k}{V}\right)\right]_{k=k_p,\omega=\omega_p}. \end{aligned}\right\} \tag{5.3}$$

Moreover, this saddle point must be a genuine pinch point of (5.1) provided that it is formed by the coalescence of k zeros from upper and lower half-planes as $\mathrm{Im}(\omega)$ is reduced to zero, and this can easily be checked by considering the behaviour of (5.1) for large $|\omega, k|$. Indeed, it follows that provided $|\epsilon V/D| \ll 1$ for $|\omega, k| \gg 1$, then the behaviour of (5.1) for large $\mathrm{Im}(\omega)$ is the same as in the dissipationless case, so that the saddle (5.3) is a genuine pinch point.

From (5.3) we can see that the real pinch point of the dissipationless dispersion relation has been destabilized by dissipation to give an absolute instability, provided that the imaginary part of ω in (5.3) is positive. For typical forms of plate dissipation it seems that $V(k_p, \omega_p) > 0$, and we therefore see that the sign of $\mathrm{Im}\omega$ depends only on the sign of $\omega_p \partial D/\partial\omega$, which is in turn the sign of the wave energy given in (4.12). We can therefore conclude that, for the forms of dissipation described above, a real pinch point corresponding to a negative-energy wave is destabilized by dissipation to give absolute instability, and that one corresponding to a positive-energy wave is stabilized.

For the cylinder problem, plate dissipation can be included by introducing a small negative imaginary part into the solid sound speed, so replacing c_p^{*2} by $c_p^{*2}(1 - \mathrm{i}\epsilon)$ with $\epsilon > 0$. In the most general case this produces a complicated form of dispersion function $V(k, \omega)$, but if we restrict attention to the case of large a and $m = O(1)$ then it follows that we can set $\tilde{m} = 0$, so that

$$V(k, \omega) = \omega^2 - (\omega - Uk)^2 \mathscr{F}(k; a) + \frac{k^2 \nu^2 \omega^2}{a^2 \left(k^2 - \frac{1}{12}\rho^2\omega^2\right)^2}. \tag{5.4}$$

Now, at $k = k_p$ on the lower branch of the dispersion curves in figure 3 we do indeed have $\omega\partial D/\partial\omega < 0$ (i.e. a negative-energy wave) provided that $a > a_2(U)$, and moreover from (5.4) $V(k_p, \omega_p) > 0$ (since as already noted $\mathscr{F}(k; a) < 0$ for all real k and m). It therefore follows that for $a > a_2(U)$ the effect of including plate dissipation will be to make the flow absolutely unstable for all U, with the absolutely unstable growth rate being proportional to ϵ; this is exactly equivalent to the result found by Abrahams & Wickham (1994) for a flat plate. For $a_3(U) < a < a_2(U)$ it appears that the pinch point $k = k_p$ corresponds to a positive-energy wave, and for $a < a_3(U)$ the pinch point does not exist anyway, so that at least from this analysis it would appear that our cylinder flow with small dissipation is not absolutely unstable for $a < a_2(U)$.

The effect of dissipation on points other than (k_p, ω_p) can also be inferred. The pinch point (k_q, ω_q) shown in figure 3(*c*) has $D_\omega(k_q, \omega_q) < 0$ and $\omega_q < 0$, and is therefore stabilized by dissipation (i.e. introducing dissipation causes the imaginary part of ω_q to become negative). With regard to the rest of the dispersion curves, we have already seen that the upper branches correspond to positive-energy waves (for instance, in figure 3*a* the upper branches joining the origin to k_a and k_b to infinity); these modes are stabilized by the introduction of dissipation. Alternatively, the lower branches of

the dispersion curves correspond to either negative-energy waves when $\omega > 0$ (for instance, the lower branch joining k_b to infinity in figure 3*a*), which are destabilized by dissipation, or to positive-energy waves when $\omega < 0$ (for instance, the lower branch in figure 3*d*, as described in §4.3), which are again stabilized by dissipation.

6. Concluding remarks

In this paper we have examined the causal motion of a fluid-loaded cylinder forced by a harmonic ring force in the presence of mean flow, and have concentrated on the case of large cylinder radius so as to assess the effects of plate transverse curvature on Crighton & Oswell's (1991) results for a flat plate. We see that the unstable motions observed by Crighton & Oswell (absolute instability for $U > U_0$ and convective instability for $U < U_0$ in $\omega < \omega_s$) are in a sense stabilized by the hoop stiffness introduced by the plate curvature – the absolute instability boundary occurs at higher flow speed (very much higher for moderate a), while convective instability will still occur for flow speeds below the absolute instability boundary but only provided that a is very large indeed (i.e. $a > a_1$). The most unusual feature of Crighton & Oswell's analysis, however, is the existence of a neutral wave with its group velocity pointing towards the driver, but again we show that plate curvature has the effect of eliminating this anomalous mode except for very large values of a. In fact, in the limit of small U we were able to deduce condition (4.5) for the existence of both convective instability and the anomalous neutral mode, which in dimensional form becomes

$$\frac{a^*}{h^*} > \left(\frac{1-\nu^2}{3}\right)^{1/2} \left(\frac{U^*}{c_p^*}\right)^{-2}. \tag{6.1}$$

Since $c_p^* \gg U^*$ in many underwater applications, it seems unlikely that this condition could ever be met for rigid plates, so that we can conclude that the usual radiation condition of outgoing waves at infinity is likely to be valid in such practical situations. (However, we also note that for compliant coatings c_p^* can be much smaller, and certainly comparable to U^*, so that the anomalous neutral mode could potentially exist in such cases.) It is interesting to note that (6.1) is independent of the fluid–solid density ratio. Crighton & Oswell also identify negative-energy waves in their flat-plate system. The anomalous mode mentioned above is in fact a negative-energy wave, but other negative-energy waves can exist in our cylindrical system down to radii which, while still large, are smaller than a_1; again for small U we found in (4.10) that negative-energy waves are present provided that, in dimensional form,

$$\frac{a^*}{h^*} > \left(\frac{8}{9}\right)^{1/3} \left(1-\nu^2\right)^{1/2} \left(\frac{\rho_s^*}{\rho_0^*}\right)^{2/3} \left(\frac{U^*}{c_p^*}\right)^{-4/3}. \tag{6.2}$$

Note here that the fluid–solid density ratio does now appear, and in such a way that the lighter the fluid loading then the greater the radius of curvature needed to observe negative-energy waves (for instance, the critical a^* for steel in air is about 80 times greater than for steel in water at the same flow speed). It should be noted that the location of the mean flow, either inside or outside the cylinder, has little effect on our results, and indeed the small-U analysis is identical for both internal and external problems. Of course, the two dispersion relations are quite different when $a = O(1)$, but our aim in this paper has been to investigate the behaviour for large a, in which case it seems that what matters is the magnitude of the transverse curvature and not its sign.

In conclusion, we can say that transverse plate curvature can have a marked

effect in modifying the flat-plate dynamics studied by previous authors. One possible extension of the present work might be to explore the whole range of possible values of azimuthal wavenumber m. Here we have restricted attention to the regime $m = O(1)$, but preliminary analysis indicates that a range of different preferred scalings of the form $m = O(U^{-\alpha})$ with $\alpha > 0$ are possible, and this will be investigated further.

The author is grateful to Professor D. G. Crighton and Dr A. D. Lucey for helpful discussions. This work was supported by the Office of Naval Research under the program in Structural Dynamics monitored by Dr G. L. Main, grant number N0014-96-1-1085.

Appendix

In this Appendix we present for completeness the equations of motion and dispersion relation for a two-dimensional fluid-loaded plate with spring foundations in the presence of mean flow, since these are closely related to our cylindrical problem in the limit of large a. It therefore follows that some of the asymptotic results derived for the cylinder apply exactly to this case, and these are summarized here.

Consider a thin elastic plate lying along the x^*-axis with mean flow of speed U^* running parallel to the x^*-axis above the plate and driven by a point force $F^*(t^*)$ at the origin. The plate equation is

$$\rho_s^* h^* \frac{\partial^2 \eta^*}{\partial t^{*2}} + B^* \frac{\partial^4 \eta^*}{\partial x^{*4}} = F^*(t^*)\delta(x^*) - p^*(x^*, t) - \lambda^* \eta^*, \tag{A 1}$$

where the bending stiffness is $B^* = c_p^{*2} h^{*3} \rho_s^*/12$ and λ^* is the dimensional spring stiffness of the spring foundation. Note that if we set $\lambda^* = 0$ then (A 1) reduces exactly to the plate equation used by Crighton & Oswell (1991). Now proceeding exactly as before, we find that the dispersion relation for this system becomes

$$-k^4 + \omega^2 + \frac{(\omega - Uk)^2}{|k|} - \frac{\lambda^* (\rho_s^* h^*)^4}{\rho_0^{*4} B^*} = 0, \tag{A 2}$$

which we can see is closely related to the dispersion relation for the cylinder in the limit of large a and small U (see e.g. equation (3.1)). By a trivial modification of the asymptotic results presented in the main body of the paper, we are therefore able to derive the following exact results for the elastic plate with spring foundations.

(a) The flow is absolutely unstable provided that U is larger than the single positive root of

$$1 = \frac{h^* \lambda^*}{c_p^{*2} \rho_s^* \rho^4} \frac{5^{5/3} 2^{8/3}}{U^{8/3}[U^{2/3} - U_0^{2/3}]}. \tag{A 3}$$

(b) If the flow is not absolutely unstable, then it will be convectively unstable over a particular range of frequencies if

$$\frac{\lambda^* h^*}{\rho_s^* c_p^{*2}} < \frac{\rho^4 U^4}{48}. \tag{A 4}$$

This is also the condition for the system to exhibit the anomalous propagation effect described by Crighton & Oswell (i.e. for there to exist a mode which possesses a negative group velocity but which is located downstream of the observer).

(c) The system will possess negative-energy waves, and therefore potentially admit

$\mathrm{Re}A_0 < 0$ for some range of frequencies, if

$$\frac{\lambda^* h^*}{c_p^{*2}\rho_s^*} < \frac{\rho^4 U^{8/3}}{2^{14/3}}. \tag{A 5}$$

Finally, following the suggestion of an anonymous referee, we note that the effects of gravity can be included in a straightforward manner. If we suppose that there is a fluid of density ρ_1^* below the plate, and that gravity acts downwards, then the effects of buoyancy would lead to an extra term $-g^*(\rho_1^* - \rho_0^*)\eta^*$ on the right-hand side of (A 1), where g^* is the acceleration due to gravity. Gravity is therefore seen to have the same effect as a spring foundation, and it therefore follows that the significant modifications to Crighton & Oswell's flat-plate results predicted for a spring foundation could also be produced by gravity.

REFERENCES

Abrahams, I. D. & Wickham, G. R. 1994 paper at EUROMECH 316, Manchester, UK.

Abramowitz, M. & Stegun, I. G. 1968 *Handbook of Mathematical Functions*. Dover.

Benjamin, T. B. 1960 Effects of a flexible boundary on hydrodynamic stability. *J. Fluid Mech.* **9**, 513–532.

Benjamin, T. B. 1963 The threefold classification of unstable disturbances in flexible surfaces bounding inviscid flows. *J. Fluid Mech.* **16**, 436–450.

Bers, A. 1983 Space-time evolution of plasma instabilities - absolute and convective. In *Handbook of Plasma Physics* (ed. M. N. Rosenbluth & R. Z. Sagdeev), vol. 1, pp. 451–517. North-Holland.

Brazier-Smith, P. R. & Scott, J. F. 1984 Stability of fluid flow in the presence of a compliant surface. *Wave Motion* **6**, 547–560.

Briggs, R. J. 1964 *Electron-stream Interaction with Plasmas*. MIT Press.

Cairns, R. A. 1979 The role of negative energy waves in some instabilities of parallel flows. *J. Fluid Mech.* **92**, 1–14.

Carpenter, P. W. & Garrad, A. D. 1985 The hydrodynamic stability of flow over Kramer-type compliant surfaces. Part 1. Tollmien-Schlichting instabilities. *J. Fluid Mech.* **155**, 465–510.

Carpenter, P. W. & Garrad, A. D. 1986 The hydrodynamic stability of flow over Kramer-type compliant surfaces. Part 2. Flow-induced surface instabilities. *J. Fluid Mech.* **170**, 199–232.

Crighton, D. G. & Oswell, J. E. 1991 Fluid loading with mean flow. I. Response of an elastic plate to localized excitation. *Phil. Trans. R. Soc. Lond.* **335**, 557–592.

Grotberg, J. B. 1994 Pulmonary flow and transport phenomena. *Ann. Review Fluid Mech.* **26**, 529–571.

Guo, Y. P. 1996 Acoustic radiation from cylindrical shells due to internal forcing. *J. Acoust. Soc. Am.* **99**, 1495–1505.

Junger, M. C. & Feit, D. 1986 *Sound, Structures, and Their Interaction*. MIT Press.

Landahl, M. T. 1962 On the stability of a laminar incompressible boundary layer over a flexible surface. *J. Fluid Mech.* **13**, 609–632.

Lighthill, M. J. 1960 Studies on magnetohydrodynamic waves and other anisotropic wave motions. *Phil. Trans. R. Soc. Lond.* **252**, 397–430.

Lucey, A. D. 1996 The excitation of waves on a flexible panel in a uniform flow. *Phil. Trans. R. Soc. Lond.* submitted.

Lucey, A. D. & Carpenter, P. W. 1992 A numerical simulation of the interaction of a compliant wall and inviscid flow. *J. Fluid Mech.* **234**, 121–146.

Scott, J. F. M. 1988 The free modes of propagation of an infinite fluid-loaded thin cylindrical shell. *J. Sound Vib.* **125**, 241–280.

Triantafyllou, G. S. 1992 Physical condition for absolute instability in inviscid hydroelastic coupling. *Phys. Fluids* **4**, 544–552.

Wu, S. F. & Maestrello, L. 1995 Responses of finite baffled plate to turbulent flow excitation *AIAA J.* **33**, 13–19.

Zhang, B. & Abrahams, I. D. 1995 The radiation of sound from a finite ring-forced cylindrical elastic shell I. Wiener-Hopf analysis. *Proc. R. Soc. Lond.* A **450**, 89–108.